

Semi-Supervised Manifold Learning with Complexity Decoupled Chart Autoencoders

Stefan C. Schonsheck ^{*}; Scott Mahan [†]; Timo Klock [‡];
Alexander Cloninger [§]; Rongjie Lai [¶]

August 24, 2022

Abstract

Autoencoding is a popular method in representation learning. Conventional autoencoders employ symmetric encoding-decoding procedures and a simple Euclidean latent space to detect hidden low-dimensional structures in an unsupervised way. This work introduces a chart autoencoder with an asymmetric encoding-decoding process that can incorporate additional semi-supervised information such as class labels. Besides enhancing the capability for handling data with complicated topological and geometric structures, these models can successfully differentiate nearby but disjoint manifolds and intersecting manifolds with only a small amount of supervision. Moreover, this model only requires a low complexity encoder, such as local linear projection. We discuss the theoretical approximation power of such networks that essentially depends on the intrinsic dimension of the data manifold and not the dimension of the observations. Our numerical experiments on synthetic and real-world data verify that the proposed model can effectively manage data with multi-class nearby but disjoint manifolds of different classes, overlapping manifolds, and manifolds with non-trivial topology.

1 Introduction

It is commonly believed that real-world data concentrates near low-dimensional structures embedded in high-dimensional space [6, 19, 31]. Therefore, detecting the hidden low-dimensional structure is a crucial step in data science, often referred to as manifold learning. Auto-encoding [9, 22, 29] is a key concept to learn low-dimensional structures from high-dimensional observations via dimensional reduction for efficient data representation in an unsupervised manner. It enables wide applications in many important tasks such as dimensional reduction [8], novel data generation [23], anomaly detection [4], molecular property prediction [28], dynamic system prediction [34] and many more [33, 7, 44, 25, 16].

Conventional autoencoders map data to a low-dimensional Euclidean domain. However, the desired continuity and invertibility of the encoder and decoder indicate that the flat geometry of the latent space is often too simple to appropriately represent a data manifold with non-trivial

^{*}University of California Davis, Department of Mathematics, TETRAPODS Institute of Data Science

[†]University of California San Diego, Department of Mathematics

[‡]DeepTech Consulting

[§]University of California San Diego, Department of Mathematics and Halicioğlu Data Science Institute

[¶]Rennselaer Polytechnic Institute, Department of Mathematics

topology. For example, it is well-known that the unit sphere in \mathbb{R}^3 is not homeomorphic to \mathbb{R}^2 —not to mention a manifold with holes, a manifold with multiple disconnected components, or intersecting manifolds. Therefore, decoded samples drawn from the simple latent space will be unlike the training distribution if the underlying distribution is concentrated on a low-dimension manifold with disconnected components, holes or overlaps [41, 31, 38].

Another important question is how to create interpretable embeddings given additionally supervised (or semi-supervised) information. This labeling can help differentiate nearby but disjoint manifolds of different classes. For example, consider simultaneously learning a dataset of handwritten digits and the labels of these digits as a function defined on the data. This distribution has intersections (or at least near intersections) if there are poorly written digits (ex: 6s and 0s that look alike). Conventional Euclidean latent representations of these intersections insist that the data be in one of these classes. However, it is more reasonable to model these points as intersection of two manifolds and treat these points as being members of each class.

In this work, we present a method for simultaneously learning manifolds and labels given semi-supervised or fully-supervised information. To overcome data manifold with complicated topology and possible nearby intersecting components, we learn the data manifold via a chart-atlas construction inspired by the chart autoencoder introduced in [38]. In addition, we present an additional mechanism to encode overlapping manifolds with different labels by incorporating semi-supervised label information. We extend this to learn data manifolds and functions thereon simultaneously. Unlike conventional autoencoders whose encoding and decoding steps share similar structures and complexity, the proposed encoding process enjoys a very low computational complexity. This asymmetric encoding-decoding procedure significantly reduces the computation cost. Theoretically, we show that such approximations can be accurately conducted with neural networks of width and depth that scale with the latent dimension of the data and only a weak dependence on the ambient dimension. Finally, we conduct numerical experiments on both synthetic and real-world data to validate the effectiveness of the proposed method.

To summarize, our main contributions are:

- We introduce a mechanism to incorporate semi-supervised information (labels) into the chart predictor/encoder. This allows for encoding overlapping manifolds with different labels;
- We explore asymmetric encoder-decoder auto-regressive modes, which save computation costs;
- We theoretically discuss the approximation power of such networks that minimizes the influence of the ambient dimension; We relax requirements on the encoder to only produce a finite distortion embedding, rather than the requirement that latent space is nearly Euclidean.

Related Work Extracting the low-dimensional structures by modeling data as being sampled from some unknown manifolds has led to many dimension reduction techniques in the past two decades [42, 37, 13, 6, 21, 46, 24, 30, 27]. Auto-encoding and variational auto-encoding [9, 22, 29, 23] are important techniques to learn low-dimensional structures in an unsupervised manner. These models’ unsupervised and oversimplified latent spaces make them insufficient to handle data with nontrivial topology, disconnected components, or multiple nearby/intersecting components.

Recently, there has been an increasing interest in introducing non-Euclidean latent space for better representation. [17] introduced a non-Euclidean latent space to guarantee the existence of a homeomorphic representation, realized by a homeomorphic variational autoencoder. However, this approach requires that the topology of the dataset is known. Similarly, several recent works [15, 36, 12] have introduced autoencoders with (hyper-)spherical or other, fixed non-euclidean latent spaces. Without assuming prior knowledge of the topological structure of the data, chart autoencoders (CAE) [38] allow for the homeomorphic representations of distributions with arbitrary topology. The

authors also show that there exists a CAE which can faithfully represent any manifold but that the number of charts may depend on the covering number of the manifold. In this work, we improve their worst-case scenario bound and prove that for many cases the number of charts needed is much lower. We further extend CAE to incorporate with semi-supervised information for detecting manifolds with overlapping structures.

It is well known that VAEs and generative adversarial networks (GANs) cannot accurately represent data from disconnected distributions [41, 31]. One crucial reason is that these models have continuous latent space and continuous layers. Therefore, data observed from separable distributions become (computationally) inseparable in the latent space. Several methods [5, 43] have been proposed to overcome this problem during data generation via rejection sampling, in which newly generated data is 'thrown out' if it doesn't close enough to resembling something from the training data. Unfortunately, this results in 'dead zones' in the latent space, which can not generate meaningful data. Similarly, other methods attempt to model the latent space using manifold learning techniques [31, 26, 35] on the latent space. However, these require more complex sampling schemes and essentially employ autoencoding as a nonlinear dimensional reduction technique. Our approach completely avoids this problem by employing compactly supported charts, which are organized via a partition of unity. As a result, we provide a more interpretable latent space and do not require any post-processing in data generation.

Many provable neural network approximation results [14, 20, 39, 10, 11] for low dimensional manifolds focus on approximating a function f supported on or near some smooth d -dimensional manifold isometrically embedded in \mathbb{R}^D with $d \ll D$. However, these results often assume the manifold is both known and well behaved. Recently, several efforts have explicitly bounded the size of networks needed to represent an unknown manifold [38] or estimate it with non-parametric methods [3]. This work improves upon these results to characterize the size of networks needed to accurately approximate manifolds with finite distortion. We show the approximation power of such networks that essentially depends on the intrinsic dimension of the data manifold. The number of charts needed to cover many manifolds is surprisingly few as shown later in Section 4.

2 Description of the Problem

We begin by describing the mathematical model of data which motivates the proposed representation. The *fuzzy manifold* hypothesis states that coherent data in high dimension concentrates *near* lower-dimensional manifold(s) [6, 31]. For example, a dataset of 256×256 natural images of k different objects rotating along a single axis in 3D will form a set of k 1D manifolds in \mathbb{R}^{256^2} . Suppose that there is some function on this data that we wish to learn. This function may be categorical (ex:labels of the picture) or continuous (ex:the rotation angle). A naive way to jointly learn the manifold and function is to concatenate the coordinate data and function values. Then one must learn the distribution in the concatenated ambient space. This problem is significantly harder due to the curse of dimensionality. Other works have attempted to solve this problem by learning a structured latent space [15, 12]. However, these approaches require problem-specific insights about the manifold's topology and the function's behavior, which are not available in many contexts. Alternatively, we propose a more computationally tractable strategy in which we factor the problem into a manifold learning problem and functional approximation problem.

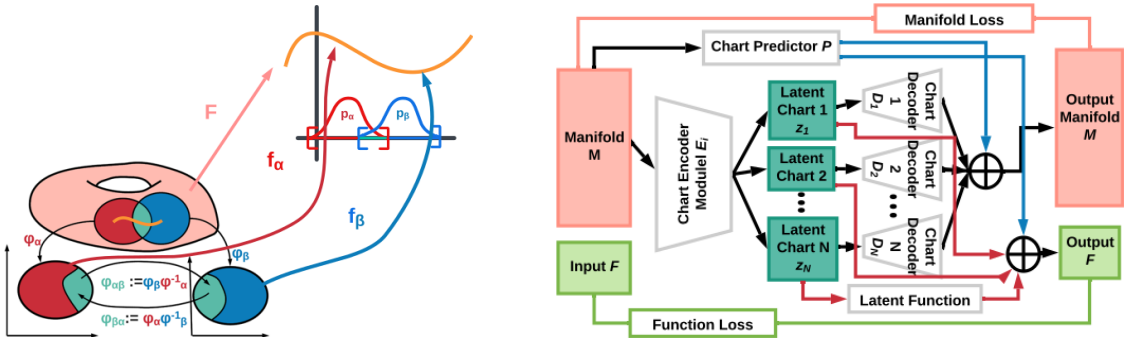


Figure 1: **Left:** Represent a function $F : \mathcal{M} \rightarrow \mathbb{R}$ from samples of F on a manifold $\mathcal{M} \subset \mathbb{R}^D$ through charts. We first parameterize \mathcal{M} with an atlas of overlapping charts $\{U_\alpha, \phi_\alpha\}_\alpha^N$, each of which is homeomorphic to \mathbb{R}^d . Then the function F can be locally approximated a chart U_α by composing function $f_\alpha : \mathbb{R}^d \rightarrow \mathbb{R}$ with ϕ_α . That is, for $x \in U_\alpha$, $F(x) \approx f_\alpha(\phi_\alpha(x))$. **Right:** Network architecture. Black lines indicate the flow of manifold data, red indicates function approximation, blue represent chart probabilities. Boxes with gray outlines represent neural modules and colored boxes represent data spaces.

We consider that data is sampled on a union of finite d -dimensional manifolds $\mathcal{M} = \cup_i \mathcal{M}_i$ in an ambient space \mathbb{R}^D . Based on a dataset sampled on \mathcal{M} and samples of a function $F : \mathcal{M} \rightarrow \mathbb{R}$, we would like to simultaneously learn the data manifold and the function thereon. We remark that F can be categorical (namely, vector valued such as a one hot encoding) in a classification problem or continuous in a regression problem. In particular, samples of values of categorical F are viewed as semi-supervised information to handle data with multi-class manifolds.

Topological Concerns Chart autoencoders (CAEs) were introduced in [38] to represent data from manifolds with non-trivial topology without prior knowledge of the topology. The authors introduce the concept of an ϵ -faithful representation, which quantitatively measures the topological and geometric approximation of autoencoders to the data manifold. An essential result of this work is that an auto-regressive model cannot accurately represent a manifold distributed dataset unless the latent space is homeomorphic to the data manifold. This motivates the use of multi-latent space models in which each chart covers only a compact portion of the data in CAE.

We improve upon previous approximation results [27, 39, 38, 2], by explicitly showing the trade-offs between the number of charts, complexity of the network, and local geometry of the manifold in the representation of a distribution concentrated near the manifold. In particular, we prove that the number of latent space charts can actually be quite small and does not need to scale with the covering number of the manifold. In some instances, the number of charts is independent of ambient dimension and the number of data points altogether. Instead, we establish a finite distortion condition that only requires the encoder to be injective. Another significant benefit of this relaxation is that it allows the encoders to be quite simple, potentially even linear projections of large pieces of the manifold. Moreover, this trade-off is shown not to affect the decoder complexity significantly.

Incorporating Supervision As an extension of the CAE model, we propose to learn manifold structure and functions thereon simultaneously. Once we have learned the local chart structure of the data manifold, we organize them via a partition of unity function, making learning F much easier. Different from conventional autoencoders which do not combine with supervised information,

this additional information can be used to improve the manifold approximation in a supervised (or semi-supervised) manner. This is an important step to handle data with multi-class nearby but disjoint manifolds. If the function to be learned is categorical, then we use constant (but learnable) functions f_α to separate the classes to learn disconnected or overlapping manifolds. By enforcing that each chart covers examples from one class of the data, we can trivially factor the problem. Then, after the model is trained, we can generate novel data from any category by sampling from the appropriate chart latent spaces. The overall mathematical model of this approximation is described in the left picture in Figure 1, where the data manifold has been parameterized by a chart structure, and a function can be viewed as composition between chart parameterization and functions on the latent space.

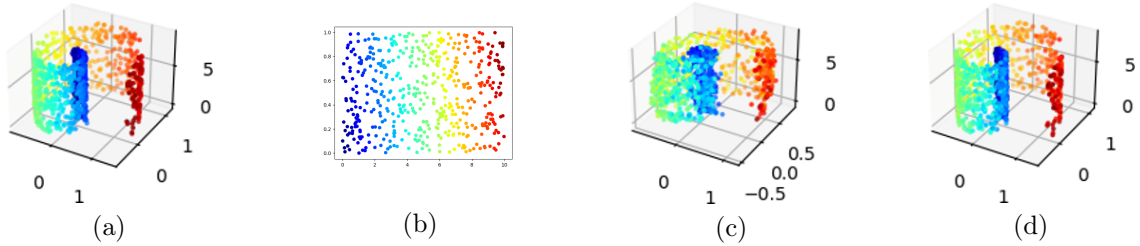


Figure 2: A function on the Swiss roll data. (a) Training Data; (b) Function on flattened data; (c) Points generated by 4D autoencoder; (d) Points generated by learning latent representation and function thereon.

One advantage of this approach is it allows for intrinsic learning of functions on the manifold other than categorical labels. Since each local approximation maps to a Euclidean latent space, we can use standard functional approximation techniques such as constant, linear, polynomial, or multilevel perceptrons to approximate the given function. Finally, by composing this approximation with the chart functions, we approximate F . Figure 2 shows a Swiss roll example of this where the ambient dimension is 3, the intrinsic dimension is 2, F maps to \mathbb{R} and is linear along certain geodesics of the manifold. It is evident that the function to be learned is linear with respect to the intrinsic metric of the manifold. For this case, learning the function in addition to the manifold only requires four more parameters than learning the manifold itself. In contrast, one naive approach to learning a representation of this data would be to concatenate the coordinates of the Swiss roll with the function data and then train an autoencoder on \mathbb{R}^4 . This requires many more parameters since the dimension of the problem is greater. One large downside to this approach occurs when the information of F is not complete—i.e. when there are points on the manifold which are unlabeled. Standard models cannot use these to train the concatenated representation. Our approach involves learning a manifold representation $\{U_\alpha, \phi_\alpha\}$ and a latent function approximation $f : \mathbb{R}^2 \rightarrow \mathbb{R}$, then approximating the $F \approx f_\alpha(\phi_\alpha)$ from the latent space. Here, we train a standard VAE on the four-dimensional data with roughly 5k parameters and a similarly sized manifold + latent function model with approximately 3k parameters. Despite being much smaller, the manifold + latent model does a better job of representing the roll’s geometry as well as the values of the function.

3 Description of Model

The overall architecture of our model is presented in the right hand side of Figure 1. Given an input point x , the encoder module, E , maps to a series of N different latent spaces Z_i , each of which is a unit cube in the desired latent dimension. The encoder module E is formed from a set of N parallel,

simple encoders E_i . In section 4 we show that these sub-modules can be very simple—even linear projections. A partition of unity function, \mathbf{p} is used to predict which latent representation should be used in the reconstruction. This function, which we dub the chart predictor, defines a probability distribution on the data allowing us to “glue” the charts together in an overlapping or disconnected manner (see examples in Figure 4). Each latent space is equipped with a decoder module that maps back to the observation space, generating a reconstruction y_i . We also define a latent function f_i , which can be combined with the encoder and partition of unity to approximate F on each chart. That is $F(x) \approx \{f_i(E_i(x)) \mid i = \arg \max_i \mathbf{p}_i(x)\}$. Given a trained model, to encode a single point we can use $\mathbf{p}(x)$ to determine which chart(s) to use for the encoding, saving us computation. Full descriptions of each of the sub-modules purposes and exact architectures for the numerical experiments are presented in A.1 and A.3.

Training, Loss and Initialization During training, each chart decoder produces an output $y_i = \mathbf{D}_i \circ \mathbf{E}_i(x)$. Then the i^{th} chart’s reconstruction error is given by: $e_i = \|x - y_i\|^2$. If x lies on the domain of only one chart, then this chart should minimize the error, if x lies in an overlapping region, then all of the overlapping charts should minimize this error. To obtain a sensible partition of unity, $\{\mathbf{p}_i\}$, we measure cross-entropy between the prediction and the inverse of the reconstruction error ($\ell_i = \text{softmax}(-e_i)$) and minimize it.

If x lies in a region of the manifold overlapped by multiple charts, then each of these charts should produce reasonable reconstructions y_i . Let $\{\alpha\}$ be the set of indices of these overlapping charts. Then each of $\{\ell_i \mid i \in \alpha\}$ should be close to zero. Hence, minimizing the cross-entropy defined above produces nearly equal probabilities for the relevant charts ($i \in \alpha$) and zero for the irrelevant ones ($i \notin \alpha$). Similarly, the function approximation loss from each chart is also weighted by \mathbf{p} to ensure that the functional loss is only propagated to the local charts. Then we have the following training loss:

$$\mathcal{L}(x) := \min_i |x - x_i|_2^2 + \lambda \sum_{i=1}^N \mathbf{p}_i \left(|x - x_i|_2^2 + \mathcal{F}(f(x), f_j(\tilde{x}_j)) + \mathcal{KL}(\mathcal{N}(\mu_i, \sigma_i), \mathcal{N}_{\frac{1}{2}, \frac{1}{4}}) \right) \quad (1)$$

where λ is a hyper-parameter, \mathcal{F} is cross-entropy loss for classification-type problems and mean square error for regression type problems, and $\mathcal{N}_{\frac{1}{2}, \frac{1}{4}}$ is the d -dimensional normal distribution centered at midpoint of the unit cube, $(\frac{1}{2})^d$, with standard deviation $\frac{1}{4}$. Note that this is a different Gaussian than standard VAEs employ since our latent spaces are compact unlike the standard VAE setup.

In order to efficiently train local representations of the data we utilize an initialization scheme to ensure that each of the chart functions initializes to different regions of the data. Then the training on the full dataset can be viewed as a region growing scheme, whereby new points are added to the domain of each chart. During training, the centers of these regions may move, and some charts may be removed. The initialization and chart removal procedure is adapted from [38] and detailed in A.2.

Data Generation After training, the model can generate novel data by sampling the latent space and then decoding the samples. To create a dataset with a distribution close to that of the training set, we first measure how often each of the charts is used in the reconstruction of the training set, as well as the distribution of points within each latent space. We then sample each of the charts proportionally to the number of times it was used in reconstruction and sample each chart with respect to the observed distribution. If the dataset has class labels, we can generate data from specific classes by sampling only from the appropriate charts. If the dataset is unlabeled, we can still generate data similar to a given an example by sampling from the latent space to which the

given sample encodes and the neighboring charts (see Figure 4). This locality property is due to the compact support of charts and is not always the case for standard VAEs and GANs [15, 38]

4 Theoretical Analysis

Low Complexity Encoder: Rather than requiring that the charts be nearly Euclidean, we simply require that each chart U_i can be encoded into a latent space bijectively with finite distortion. This allows us to reduce the number of charts needed, from a covering number that scales exponentially with the intrinsic dimension to a small number of charts independent of the intrinsic dimension in certain circumstances [39, 2]. This relaxed assumption also allows us to use much more simple functions to perform the encoding operation than previous approaches. This encoding can even be a linear projection if the manifold has a finite distortion embedding. Meanwhile, each decoder D_i can then be approximated with a ReLU network whose complexity depends only weakly on the ambient dimension D .

Definition 1. An atlas $\{(U_i, \phi_i)\}_{i=1}^n$ is a **finite distortion embedding** of \mathcal{M} if each chart function $\phi_i : U_i \rightarrow \mathbb{R}^d$ is bi-Lipschitz.

The generality of this finite distortion condition also allows us to use a relatively small number of charts. Later, we state and prove a somewhat restrictive but easily checked condition that guarantees a finite distortion embedding of \mathcal{M} . We also conjecture an intuitive, more general sufficient condition for a finite distortion embedding that is more difficult to confirm for real-world data.

Chart Reach Condition We characterize the regularity of a given atlas parameterization by measuring the reach of each chart. Defined originally in [18] and discussed at length in Appendix B.1, the reach of a manifold \mathcal{M} is the largest number $\tau_{\mathcal{M}}$ such that every point within distance $\tau_{\mathcal{M}}$ of \mathcal{M} has a unique nearest neighbor on \mathcal{M} . This measure depends on the curvature and smoothness of the manifold and how close the manifold is to self-intersecting. Thus, the reach of each chart gives us a bound on how many charts are needed for a finite distortion embedding of \mathcal{M} . Formally, we have the following result, the proof of which is delayed to B.1.

Theorem 1. Let $\delta > 0$. Suppose each $U_i \subset \mathcal{M} \subset \mathbb{R}^D$ is a connected submanifold such that $\|u_1 - u_2\| \leq 2\tau_{U_i} - \delta$ for all $u_1, u_2 \in U_i$. Then for each U_i there is a d -dimensional affine space $\mathcal{H}_i \subset \mathbb{R}^D$ such that the projection map $\pi_{\mathcal{H}_i} : U_i \rightarrow \mathcal{H}_i$ is bi-Lipschitz with lower Lipschitz constant $(1 + (D - d)\frac{2\tau_{U_i}}{\delta})^{-1/2}$.

Theorem 1 gives a sufficient condition for $\{(U_i, \pi_{\mathcal{H}_i})\}_{i=1}^n$ to be a finite distortion embedding of \mathcal{M} . The reach of each chart has an intuitive geometric meaning and can often be calculated exactly for simple manifolds or approximated computationally for more complex ones [1, 40]. Below, we provide an example where the condition in Theorem 1 describes the exact number of charts needed for a finite distortion embedding.

Example 1: Let $\mathcal{M} = \mathcal{S}^1 \subset \mathbb{R}^2$. In polar coordinates, $\mathcal{S}^1 = \{s = (r, \theta) \mid r = 1, \theta \in [0, 2\pi)\}$. Define the charts $U_1 = \{s \in \mathcal{S}^1 \mid \theta \in (-\frac{\pi}{3} - \epsilon, \frac{\pi}{3} + \epsilon)\}$, $U_2 = \{s \in \mathcal{S}^1 \mid \theta \in (\frac{\pi}{3} - \epsilon, \pi + \epsilon)\}$, and $U_3 = \{s \in \mathcal{S}^1 \mid \theta \in (-\pi - \epsilon, -\frac{\pi}{3} + \epsilon)\}$ for $\epsilon > 0$. Consider $s_1 = (1, \frac{\pi}{3})$ and $s_2 = (1, -\frac{\pi}{3})$ in \mathcal{S}^1 . Then $\|s_1 - s_2\| = 2\sin(\pi/3) = \sqrt{3}$ in \mathbb{R}^2 . While s_1 and s_2 are not the farthest apart points in U_1 , given any $\eta > 0$ we can choose ϵ small enough so that $\|u_1 - u_2\| < \sqrt{3} + \eta$ for all $u_1, u_2 \in U_1$. The reach of each chart U_i is $\tau_{U_i} = 1$. Thus, each U_i satisfies the assumption of Theorem 1 with $\delta = 0.25$ for ϵ small enough. The chart U_1 can be linearly projected onto the space $\mathcal{H}_1 = \{(0, y) \in \mathbb{R}^2 \mid y \in \mathbb{R}\}$ via the map $\pi_{\mathcal{H}_1}(x, y) = y$, as shown in Figure 3. This projection is clearly injective and bi-Lipschitz,

and similar maps exist for U_2 and U_3 . Thus, this choice of charts admits a finite distortion embedding of \mathcal{M} .

Note that in this example, we can find a finite distortion embedding if and only if each chart has an arc length less than π . As soon as the arc length of a chart U_i exceeds π , we can choose two antipodal points $u_1, u_2 \in U_i$ such that $\|u_1 - u_2\| = 2\tau_{U_i} = 2$, so the condition of Theorem 1 is not satisfied. Moreover, U_i cannot be injectively projected onto a linear subspace. Hence, in this example, the condition of Theorem 1 coincides exactly with the existence of a finite distortion embedding.

Normal Vector Characterization: Theorem 1 only provides a sufficient condition for the manifold to have a finite distortion embedding. In reality, there is a much larger class of manifolds, both smooth and non-smooth, that have finite distortion embeddings. Moreover, we can often reduce the number of charts below the number required by Theorem 1 and still obtain a finite distortion embedding.

Example 2: Let $\mathcal{M} \subset \mathbb{R}^2$ be a triangle with sides T_1, T_2 , and T_3 , where

$$T_1 = \{(x, 0) \mid x \in [-1, 1]\}, \quad T_2 = \{(x, x + 1) \mid x \in [-1, 0]\}, \quad T_3 = \{(x, 1 - x) \mid x \in [0, 1]\}.$$

If we allow closed charts, we can choose $U_i = T_i$ so that each chart has infinite reach (being just a line segment). These charts satisfy Theorem 1 and each side of the triangle is already contained in an affine subspace of \mathbb{R}^2 . However, if we ignore the requirements of Theorem 1 we can get a finite distortion embedding of \mathcal{M} with only 2 charts. In particular, set $U_1 = T_1$ and $U_2 = T_2 \cup T_3$ with the projection map $\pi_{U_2}(x, y) = x$, as shown in Figure 3. These charts clearly admit a finite distortion embedding, but they do not satisfy the assumptions of Theorem 1 since $\tau_{U_2} = 0$.

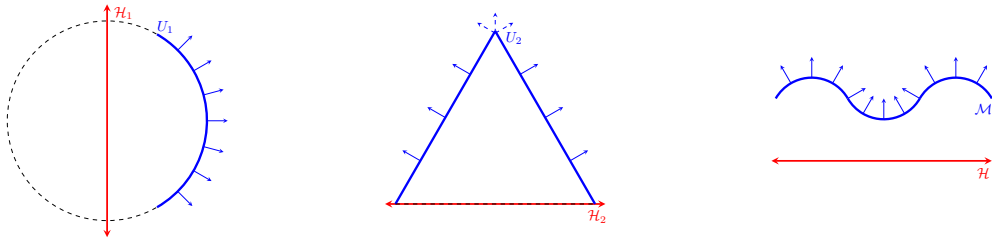


Figure 3: Example choices of charts that admit a finite distortion embedding of a 1-dimensional manifold $\mathcal{M} \subset \mathbb{R}^2$. In each case, the normal vectors of each chart all lie in the same half space.

Motivated by Figure 3, we propose a more general condition for a finite distortion embedding that places requirements on the Gauss map of each chart. The Gauss map gives a mapping from every point on a surface to its corresponding normal vector, which generates an embedding onto the unit sphere. Our conjecture characterizes a finite distortion embedding by the existence of a half-space that contains the image of the Gauss map for each chart.

Conjecture 1. Let \mathcal{M} be a smooth orientable $(D-1)$ -dimensional manifold in \mathbb{R}^D . Suppose for each chart U_i there exists $n_i \in \mathbb{R}^D$ such that $\langle n_i, N_i(u) \rangle \geq \delta > 0$ for all $u \in U_i$, where $N_i : U_i \rightarrow \mathcal{S}^{D-1}$ is the Gauss map of U_i . Then $\{(U_i, \pi_{\mathcal{H}_i})\}_{i=1}^n$ gives a finite distortion embedding of \mathcal{M} , where $\mathcal{H}_i = \{x \in \mathbb{R}^D \mid \langle n_i, x \rangle = 0\}$.

We believe Conjecture 1 can be generalized to non-smooth manifolds by including a notion of “supnormal” vectors. A vector \mathbf{v} at a non-differentiable point x_0 is sup-normal if $\mathbf{v}^\perp \cap N_{\mathcal{M}}(x_0) = \{x_0\}$ for a sufficiently small open neighborhood $N_{\mathcal{M}}(x_0)$ of x_0 on \mathcal{M} (as illustrated by the the dashed

arrows at the top of the triangle in Figure 3). Additionally, the Gauss map can be generalized to d -dimensional submanifolds of \mathbb{R}^D . These more general conditions conjectured above are a part of current and future work.

Decoder Complexity The complexity of auto-encoding a manifold generally depends on the topological and geometric properties of the manifold. By choosing charts with simple topology, we can use linear encoders and low-complexity decoders for this task. In particular, each decoder can be approximated by a ReLU network whose complexity depends mainly on the distortion of the decoder function and only weakly on the ambient dimension D .

Theorem 2. *Let $\{(U_i, \phi_i)\}_{i=1}^n$ be a finite distortion embedding of \mathcal{M} . Then for each decoder $D_i = \phi_i^{-1}$ and any $\epsilon \in (0, 1)$, there is a ReLU network $\hat{D}_i : \mathbb{R}^d \rightarrow \mathbb{R}^D$ such that*

1. $\|D_i - \hat{D}_i\|_\infty < \epsilon$;
2. \hat{D}_i has at most $c \ln(1/\epsilon)$ layers and $c\epsilon^{-d} \ln(1/\epsilon)$ computation units followed by a single matrix multiplication of size $D \times c\epsilon^{-d}$, for some constant $c = c(d)$.

The proof of Theorem 2 is presented in B.2. This theorem shows that we can approximate each decoder with a low-complexity neural network. In particular, all layers except for the final one are independent of the manifold data and its ambient dimension; they only serve to make a fine enough partition of the latent space. The final matrix multiplication consists of a finite number of decoded points to embed the data into \mathbb{R}^D . This network architecture is similar to a multidimensional version of the construction presented in [45].

In practice, we cannot directly implement the network \hat{D}_i in Theorem 2 because we do not have access to the true decoder D_i , which determines the weights of the final layer. Our goal now is to approximate each decoder $D_i : [0, 1]^d \rightarrow \mathbb{R}^D$ given noisy samples $\{z_j, x_j\}_{j=1}^n$. Given this sample, we approximate D_i using a sum-product of a partition of unity with constant terms of vector-valued local polynomial regression functions. The result is an approximator that can be implemented by a ReLU network with weights dependent on known sample data, and whose convergence rate is independent of D . Combining the local polynomial regression convergence rates from [2] with a fine enough partition of unity gives the following result, the proof of which is presented in B.3.

Theorem 3. *Let $\{(U_i, \phi_i)\}_{i=1}^n$ be a finite distortion embedding of \mathcal{M} with $D_i = \phi_i^{-1} \in C^k([0, 1]^d)$. Let $\{z_j, x_j\}_{j=1}^n$ be a sample satisfying the assumptions described in Appendix B.3, and define the approximation $\hat{D}_{i,n}$ analogous to Equation (14) in Appendix B.3. Then for any $\epsilon > 0$ there are C and n large enough so that*

$$P(2^d \cdot \|D_i - \hat{D}_{i,n}\|_\infty > Cn^{-\frac{k}{2k+d}} + C\sqrt{d}) \leq \epsilon.$$

Given a large enough sample size n , Theorem 3 implies that we can approximate the decoder D_i to a certain degree of accuracy with high probability, using just the sample data. We can then in turn approximate this local regression function with a ReLU network as in Appendix B.2, yielding a network that approximates D_i and can be implemented in practice.

5 Experimental Results

This section presents numerical experiments on synthetic and real-world data in supervised, semi-supervised, and unsupervised settings. Complete model and training descriptions are given in the appendix A.3. All code used to generate this data will be included in the supplementary material.

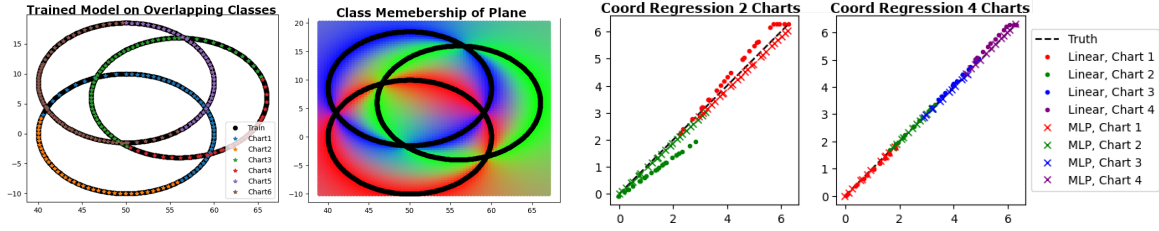


Figure 6: Left: Overlapping circle training data and reconstruction. Right: Chart prediction evaluated on the plane.

Figure 7: Regression of Angles in Coil with 2 and 4 chart models using linear and MLP latent function modules

Unsupervised Geometric examples. We begin with illustrative synthetic experiments that demonstrate the efficacy of learning manifolds and functions. Figure 4 illustrates learning disconnected, non-smooth manifolds with finite distortion. Each chart only covers part of one of the triangles, while their union covers the entire training set. Once the model is trained, we can cluster the charts by examining the confusion matrix of outputs shown in Figure 4. To form this matrix, we uniformly sample the latent space of each chart, then measure the chart prediction activation of the other charts on this synthetic data. From the confusion matrix, we see that charts 1 and 2 overlap to cover one component and charts 3,4 and 5 cover the other component. We can generate data of a particular class by sampling only from the appropriate charts.

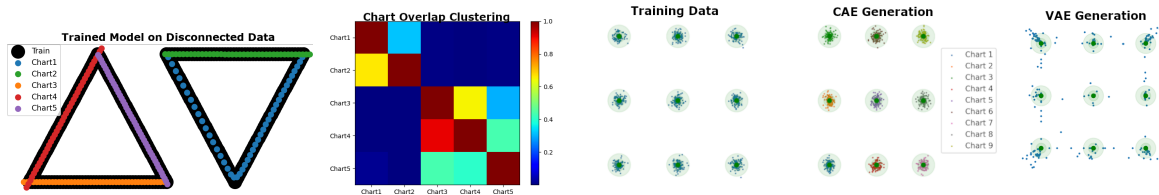


Figure 4: Left: Triangle training and reconstruction. Right: Chart overlaps via confusion clustering.

Figure 5: Left: Training data, Middle: Sampling from trained model. Right: Sampling from trained VAE.

The example in Figure 5 shows a model with a 2D latent space trained on data drawn from 9 disconnected Gaussian distributions. We initialize with 12 charts and use the chart removal procedure [38] during training to reduce the number needed in the final representation to 9. We observe that the charts are disconnected and that the model can appropriately generate novel data by sampling the learned distribution. We emphasize that these samples are taken directly from the model and that there is no rejection sampling scheme in use. As a comparison, it is clear to see that conventional VAEs will generate data in between the disconnected components since their latent space is a connected Euclidean domain. Our method performs extremely well for generating data sampled from disconnected distributions.

Supervised and Semi-Supervised Problems. In this example, we show how functional information, such as class labels, can be used in conjunction with manifold learning to handle the case of overlapping manifolds. In Figure 6, the dataset is made of three mutually overlapping and labeled

circles. By using a multi-chart model with a one-dimensional latent space and constant (but learnable) latent functions, we successfully separate the data into three classes, each covered by two charts.

Next, we present results using a semi-supervised scheme on a real-world dataset. The Coil-10 dataset [32, 31] contains images of 10 physical objects rotating along one axis in 3D. This dataset can be modeled as 10 circles embedded in a high dimension ambient space. The difficulty in properly representing this dataset is that the minimum pixel distance between some of the classes is smaller than the maximum pixel distance within the class. Variation autoencoders, GANs and the original chart autoencoder all fail to properly represent the disconnected nature of this data-set. Divide-and-conquer methods struggle since the separation between the classes is very small. However, using only ten percent of the labels in a semi-supervised regime, we are able to successfully disentangle the dataset into 10 manifolds, each represented with two charts. As results, interpolation shown in Figure 8 illustrates that the proposed method successfully capture the overlapped data manifold structure.

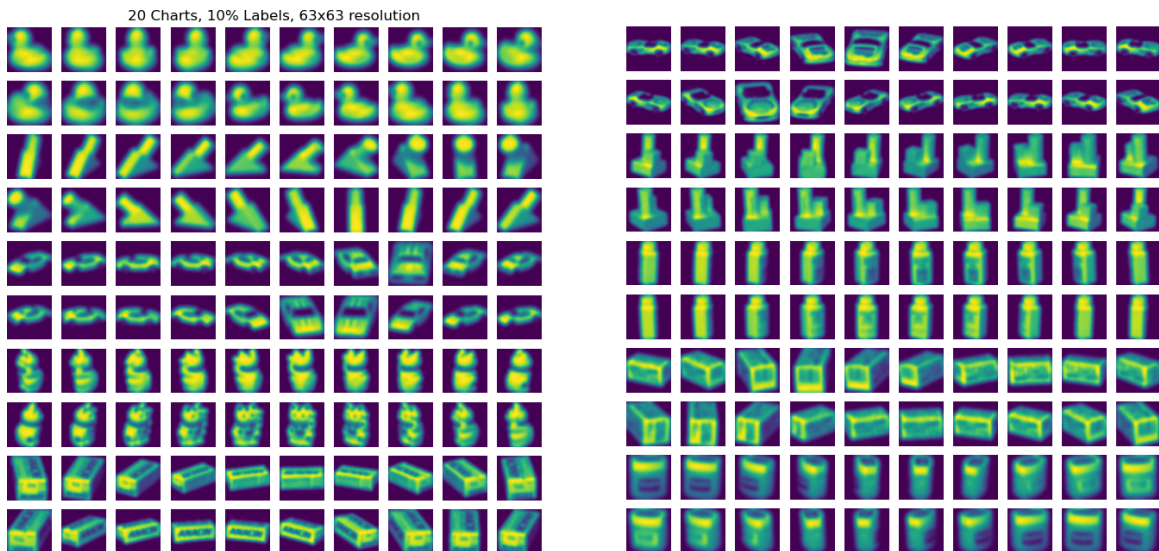


Figure 8: Sampling the latent space of a 20-chart CAE on Coil-10. Each row represents a single chart and charts are rearranged into class groups

In a second experiment on this dataset, we focus on one class and train the latent function to approximate the angle of the object’s rotation. We repeat this experiment using linear and 3-layer MLP latent function models. From the results in Figure 7, we see that the more complex latent models do a better job of predicting the angle since they are better able to counteract the distortion of the linear encoder. This numerical result supports the theory developed in section 4.

6 Conclusion

In this work, we have proposed a chart auto-encoder that can incorporate additional information such as class labels to detect hidden low-dimensional manifold structures in a semi-supervised manner. The proposed asymmetric encoding-decoding process enjoys a very low complexity encoder, such as local linear projection. Meanwhile, it allows us to learn representations for manifolds with highly nontrivial topology, including manifolds with holes, disconnected manifolds. In addition, it can

successfully differentiate nearby but disjoint manifolds and intersecting manifolds with only a small amount of supervision. Theoretically, we show that such approximations can be accurately conducted with neural networks of width and depth that scale with the intrinsic dimension of the data and only a weak dependence on the ambient dimension. Our numerical experiments on synthetic and real-world data demonstrate the effectiveness of the proposed method. Future work may involve approximating more complicated processes, such as dynamical systems, on manifolds, or adopting this chart auto-encoder to other generative models, such as adversarial networks or diffusion networks.

7 Acknowledgements

S.C. Schonscheck’s work is partially supported by the US National Science Foundation grant DMS-1912747. A Clonigers’s work is partially supported by NSF DMS-1818945, DMS- 2012266, and Intel research. R. Lai’s work is supported in part by an NSF CAREER Award (NSF DMS 1752934) and NSF DMS-2134168.

References

- [1] Eddie Aamari, Jisu Kim, Frédéric Chazal, Bertrand Michel, Alessandro Rinaldo, and Larry Wasserman. Estimating the reach of a manifold. *Electronic journal of statistics*, 13(1):1359–1399, 2019.
- [2] Yariv Aizenbud and Barak Sober. Convergence rates of vector-valued local polynomial regression. *arXiv preprint arXiv:2107.05852*, 2021.
- [3] Yariv Aizenbud and Barak Sober. Non-parametric estimation of manifolds from noisy data. *arXiv preprint arXiv:2105.04754*, 2021.
- [4] Jinwon An and Sungzoon Cho. Variational autoencoder based anomaly detection using reconstruction probability. *Special Lecture on IE*, 2(1):1–18, 2015.
- [5] Samaneh Azadi, Catherine Olsson, Trevor Darrell, Ian Goodfellow, and Augustus Odena. Discriminator rejection sampling. In *International Conference on Learning Representations*, 2019.
- [6] Mikhail Belkin and Partha Niyogi. Laplacian eigenmaps for dimensionality reduction and data representation. *Neural Computation*, 15(6):1373–1396, 2003.
- [7] Yoshua Bengio, Aaron Courville, and Pascal Vincent. Representation learning: a review and new perspectives. *IEEE Transactions on Pattern Analysis and Machine Intelligence*, 35(8):1798–1828, 2013.
- [8] Yoshua Bengio, Ian J Goodfellow, and Aaron Courville. Deep learning. *Nature*, 521:436–444, 2015.
- [9] Hervé Bouchard and Yves Kamp. Auto-association by multilayer perceptrons and singular value decomposition. *Biological Cybernetics*, 59(4-5):291–294, 1988.
- [10] Minshuo Chen, Haoming Jiang, Wenjing Liao, and Tuo Zhao. Efficient approximation of deep relu networks for functions on low dimensional manifolds. In *Advances in Neural Information Processing Systems*, pages 8172–8182, 2019.

- [11] Alexander Cloninger and Timo Klock. A deep network construction that adapts to intrinsic dimensionality beyond the domain. *Neural Networks*, 141:404–419, 2021.
- [12] Marissa Connor and Christopher Rozell. Representing closed transformation paths in encoded network latent space. *arXiv preprint arXiv:1912.02644*, 2019.
- [13] T.F. Cox and M.A.A. Cox. *Multidimensional scaling*. Chapman and Hall, 2001.
- [14] Balázs Csanád Csáji et al. Approximation with artificial neural networks. *Faculty of Sciences, Eötvös Loránd University, Hungary*, 24(48):7, 2001.
- [15] Tim R Davidson, Luca Falorsi, Nicola De Cao, Thomas Kipf, and Jakub M Tomczak. Hyper-spherical variational auto-encoders. *arXiv preprint arXiv:1804.00891*, 2018.
- [16] Nicolas Donati, Abhishek Sharma, and Maks Ovsjanikov. Deep geometric functional maps: Robust feature learning for shape correspondence. In *Proceedings of the IEEE/CVF Conference on Computer Vision and Pattern Recognition*, pages 8592–8601, 2020.
- [17] Luca Falorsi, Pim de Haan, Tim R Davidson, Nicola De Cao, Maurice Weiler, Patrick Forré, and Taco S Cohen. Explorations in homeomorphic variational auto-encoding. *arXiv preprint arXiv:1807.04689*, 2018.
- [18] Herbert Federer. Curvature measures. *Transactions of the American Mathematical Society*, 93(3):418–491, 1959.
- [19] Charles Fefferman, Sanjoy Mitter, and Hariharan Narayanan. Testing the manifold hypothesis. *Journal of the American Mathematical Society*, 29(4):983–1049, 2016.
- [20] László Györfi, Michael Kohler, Adam Krzyzak, and Harro Walk. *A distribution-free theory of nonparametric regression*. Springer Science & Business Media, 2006.
- [21] Xiaofei He and Partha Niyogi. Locality preserving projections. In *NIPS*, 2003.
- [22] Geoffrey E Hinton and Richard S Zemel. Autoencoders, minimum description length and helmholtz free energy. In *Advances in neural information processing systems*, volume 7, pages 3–10, 1994.
- [23] Diederik P Kingma and Max Welling. Auto-encoding variational bayes. *arXiv preprint arXiv:1312.6114*, 2013.
- [24] E. Kokiopoulou and Y. Saad. Orthogonal neighborhood preserving projections: a projection-based dimensionality reduction technique. *IEEE Transactions on Pattern Analysis and Machine Intelligence*, 29(12):2143–2156, 2007.
- [25] Matt J Kusner, Brooks Paige, and José Miguel Hernández-Lobato. Grammar variational autoencoder. In *International conference on machine learning*, pages 1945–1954. PMLR, 2017.
- [26] Henry Li, Ofir Lindenbaum, Xiuyuan Cheng, and Alexander Cloninger. Variational diffusion autoencoders with random walk sampling. In *European Conference on Computer Vision*, pages 362–378. Springer, 2020.
- [27] Wenjing Liao and Mauro Maggioni. Adaptive geometric multiscale approximations for intrinsically low-dimensional data. *J. Mach. Learn. Res.*, 20:98–1, 2019.

- [28] Jaechang Lim, Seongok Ryu, Jin Woo Kim, and Woo Youn Kim. Molecular generative model based on conditional variational autoencoder for de novo molecular design. *Journal of cheminformatics*, 10(1):1–9, 2018.
- [29] Cheng-Yuan Liou, Wei-Chen Cheng, Jiun-Wei Liou, and Daw-Ran Liou. Autoencoder for words. *Neurocomputing*, 139:84–96, 2014.
- [30] Laurens van der Maaten and Geoffrey Hinton. Visualizing data using t-sne. *Journal of Machine Learning Research*, 9(Nov):2579–2605, 2008.
- [31] Gal Mishne, Uri Shaham, Alexander Cloninger, and Israel Cohen. Diffusion nets. *Applied and Computational Harmonic Analysis*, 47(2):259–285, 2019.
- [32] Sameer A Nene, Shree K Nayar, Hiroshi Murase, et al. Columbia object image library (coil-100). *Technical Report No. CUCS-006-96*, 1996.
- [33] Andrew Ng et al. Sparse autoencoder. *CS294A Lecture notes*, 72(2011):1–19, 2011.
- [34] Samuel E Otto and Clarence W Rowley. Linearly recurrent autoencoder networks for learning dynamics. *SIAM Journal on Applied Dynamical Systems*, 18(1):558–593, 2019.
- [35] Adityanarayanan Radhakrishnan, Karren Yang, Mikhail Belkin, and Caroline Uhler. Memorization in overparameterized autoencoders. *arXiv preprint arXiv:1810.10333*, 2018.
- [36] Luis Armando Pérez Rey. Disentanglement with hyperspherical latent spaces using diffusion variational autoencoders. *Proceedings of Machine Learning Research*, 1:1–4, 2019.
- [37] Sam T Roweis and Lawrence K Saul. Nonlinear dimensionality reduction by locally linear embedding. *Science*, 290(5500):2323–2326, 2000.
- [38] Stefan Schonsheck, Jie Chen, and Rongjie Lai. Chart auto-encoders for manifold structured data. *arXiv preprint arXiv:1912.10094*, 2019.
- [39] Uri Shaham, Alexander Cloninger, and Ronald R Coifman. Provable approximation properties for deep neural networks. *Applied and Computational Harmonic Analysis*, 44(3):537–557, 2018.
- [40] P Suárez-Serrato. Turing approximations, toric isometric embeddings & manifold convolutions. *arXiv preprint arXiv:2110.02279*, 2021.
- [41] Ugo Tanielian, Thibaut Issenhuth, Elvis Dohmatob, and Jeremie Mary. Learning disconnected manifolds: a no gan’s land. In *International Conference on Machine Learning*, pages 9418–9427. PMLR, 2020.
- [42] Joshua B Tenenbaum, Vin De Silva, and John C Langford. A global geometric framework for nonlinear dimensionality reduction. *Science*, 290(5500):2319–2323, 2000.
- [43] Ryan Turner, Jane Hung, Eric Frank, Yunus Saatchi, and Jason Yosinski. Metropolis-Hastings generative adversarial networks. In Kamalika Chaudhuri and Ruslan Salakhutdinov, editors, *Proceedings of the 36th International Conference on Machine Learning*, volume 97 of *Proceedings of Machine Learning Research*, pages 6345–6353. PMLR, 09–15 Jun 2019.
- [44] Haowen Xu, Wenxiao Chen, Nengwen Zhao, Zeyan Li, Jiahao Bu, Zhihan Li, Ying Liu, Youjian Zhao, Dan Pei, Yang Feng, et al. Unsupervised anomaly detection via variational auto-encoder for seasonal kpis in web applications. In *Proceedings of the 2018 world wide web conference*, pages 187–196, 2018.

- [45] Dmitry Yarotsky. Error bounds for approximations with deep ReLU networks. *Neural Networks*, 94:103–114, 2017.
- [46] Zhenyue Zhang and Hongyuan Zha. Principal manifolds and nonlinear dimensionality reduction via tangent space alignment. *SIAM Journal on Scientific Computing*, 26(1):313–338, 2004.

A Model Description

A.1 Description of Submodules

Encoder and Decoder We parameterize the chart functions $\{\phi_i\}$ and their inverses with multilevel perceptrons. The encoder module, E , maps input data to N compact latent spaces. That is, $E : x \in \mathcal{M} \subset \mathbb{R}^D \rightarrow \{\mu, \sigma\}_{i=1}^N \in \mathbb{R}[0, 1]^d \oplus \mathbb{R}[0, 1]^d$. Each of these latent spaces, or chart spaces, is equipped with its own decoder which maps from the latent space back to the data manifold $D_i : z_i \in M_i \subset \mathbb{R}^D$.

In traditional autoencoder frameworks, the encoder and decoder are often thought of as being approximate inverses of each other, and have symmetric architecture. However, this is unnecessary in our approach due to the chart prediction function. Section 4 gives an more detailed explanation of this, and numeric results in section 5 show that even linear encoders can be used to encode complex non-linear data. The key insight here is that as long as the encoder maps with finite distortion, local PCA provides a good enough approximation of the manifold that we can learn the exponential map (via the decoder). Since each of these decoders only has to decode a small portion of the entire manifold, they can be much simpler than the global decoders more commonly used.

Latent Space The so called ‘reparameterization trick’ [23] is used in variational autoencoders to ensure that the data is ‘nicely’ distributed in the latent space. We adapt this idea to encourage the distributions within each chart to be concentrated near the center of the chart space. Then, rather than directly outputting a latent variable z_i for the i^{th} chart space, the encoder will instead predict a Gaussian distribution in the space parameterized by the output μ_i, σ_i . Then, before the decoding process the latent variable is sampled from this distribution.

Chart Predictor Since the encoder model produces a latent representation of a given data point in each chart space we must choose which of the charts to use for reconstruction of said point. To do so we build a partition of unity over the data manifold. This can be achieved with a neural network ending in a soft max layer: $P : x_i \rightarrow p \in \Omega$. When working with continuous datasets we weight the output of each chart by the value p , and for disconnected datasets we simply choose the chart with the largest p values.

Function Approximation To approximate a function F on the manifold we use a function defined on the chart space. Each chart is equipped with a $f_i : z_i \rightarrow \hat{x}_i \in \mathbb{R}$. Depending on the application f may be parameterized as a constant function, polynomial basis or neural network. If functional data is only available on some subset of the training data (i.e. the labels are incomplete) we only run this module on those data points.

A.2 Initialization

In order to efficiently train local representations of the data we propose an initialization scheme to ensure that each of the chart functions initializes to different regions of the data. To train an N -chart model, given some training data $x \in \mathcal{M}$ with functional samples $f(x)$, we first perform farthest point k-means sampling on the lifted varifold $\mathcal{P} = \mathcal{M} \oplus f(\mathcal{M})$ to obtain N well distributed initialization points $\{\tilde{x}_j\}_{j=1}^N$. We then assign one of these points to each of the N charts and train them to reconstruct the assigned point, with the latent representation at the center of the latent space. Note that since we represent the latent space of each chart as a unit hypercube $\mathbb{R}^d[0, 1]$,

this center is the vector $\frac{1}{2}$. We also use these points to pre-train the chart prediction module. The initialization loss is:

$$\mathcal{L}(x) := \sum_{j=1}^N \left(|E(x)_j - \frac{1}{2}|_2^2 + |D_j(\frac{1}{2}) - \tilde{x}_j|_2^2 + |p_j - \delta_j|_2^2 + \mathcal{F}(f(x), f_j(\tilde{x}_j)) \right) \quad (2)$$

With this in mind, we can think of training on the full dataset as a region growing scheme, whereby new points are added to the domain of each chart. However, we stress that during training the centers of these regions may move. Moreover, by employing the chart removal process detailed in [38] we can simplify the representation by eliminating charts that only cover a small portion of the data, or one for which the nearby charts are already doing a good job of representing.

A.3 Architecture Details for Numerical Results

Single Chart CAE- Figure 2

Number of charts = 1

Chart Encoder : $x \rightarrow FC_{10} \rightarrow (FC_d, FC_d) \rightarrow z_\alpha, \sigma_\alpha$

Chart Decoders : $z_\alpha \rightarrow FC_{10} \rightarrow FC_{10} \rightarrow FC_{2d} \rightarrow y_\alpha$

Linear Latent Modules : $z \rightarrow FC_1 \rightarrow f$

Chart Prediction : $x \rightarrow FC_{10} \rightarrow FC_{10} \rightarrow FC_N \rightarrow softmax \rightarrow p$

Geometric CAE- Figures 4,5,6

Number of charts = 5, 6, 12

Chart Encoder : $x \rightarrow FC_{10} \rightarrow (FC_d, FC_d) \rightarrow z_\alpha, \sigma_\alpha$

Chart Decoders : $z_\alpha \rightarrow FC_{10} \rightarrow FC_{10} \rightarrow FC_{2d} \rightarrow y_\alpha$

Constant Latent Modules : $z_\alpha \rightarrow f_\alpha$

Chart Prediction : $x \rightarrow FC_{10} \rightarrow FC_{10} \rightarrow FC_N \rightarrow softmax \rightarrow p$

Coil-10 CAE- Figure 8

Number of charts = 20

Chart Encoder : $x \rightarrow FC_{100} \rightarrow (FC_d, FC_d) \rightarrow z_\alpha, \sigma_\alpha$

Chart Decoder : $z_\alpha \rightarrow Conv_{3,3,16,8} \rightarrow Conv_{3,3,8,8} \rightarrow Conv_{3,3,8,1} \rightarrow y_\alpha, \sigma_\alpha$

Constant Latent Modules : $z_\alpha \rightarrow f_\alpha$

Chart Prediction : $z \rightarrow FC_{100} \rightarrow FC_{100} \rightarrow softmax \rightarrow p$

Coil-1 with angle regression CAE- Figure 7

Number of charts = 2, 4

Chart Encoder : $x \rightarrow (FC_1, FC_1) \rightarrow z_\alpha, \sigma_\alpha$

Chart Decoder : $z_\alpha \rightarrow Conv_{3,3,16,64} \rightarrow Conv_{3,3,64,8} \rightarrow Conv_{3,3,8,1} \rightarrow FC_m \rightarrow y_\alpha$

Linear Latent Modules : $z \rightarrow FC_1 \rightarrow 2\pi * sigmoid \rightarrow f_\alpha$

MLP Latent Modules : $z \rightarrow FC_{10} \rightarrow FC_{10} \rightarrow FC_2 \rightarrow 2\pi * sigmoid \rightarrow f_\alpha$

Chart Prediction : $z \rightarrow FC_{100} \rightarrow FC_{100} \rightarrow softmax \rightarrow p$

B Theory and Proofs

B.1 Proof of Theorem 1

We first define the reach of a set. In what follows, let $\langle \cdot, \cdot \rangle$ denote the standard Euclidean inner product on \mathbb{R}^D and $\|\cdot\|$ denote the associated norm. Given a closed set $X \subset \mathbb{R}^D$ and a point $z \in \mathbb{R}^D$, let $d(z, X) = \inf_{x \in X} \|z - x\|$ denote the distance from z to X . The medial axis $\text{Med}(X)$ of X is defined as the set of points in \mathbb{R}^D that have at least two nearest neighbors in X :

$$\text{Med}(X) = \{z \in \mathbb{R}^D \mid \text{there exist } x \neq y \in X \text{ such that } \|x - z\| = \|y - z\| = d(z, X)\}.$$

The reach τ_X of X is then defined as the distance from X to $\text{Med}(X)$:

$$\tau_X = d(X, \text{Med}(X)) = \inf_{x \in X} d(x, \text{Med}(X)) = \inf_{z \in \text{Med}(X)} d(X, z).$$

The reach of a set has an intuitive geometric meaning. It can be described as the radius of the largest ambient ball that can be freely “rolled around” the set. This intuition is illustrated in Figure 9.

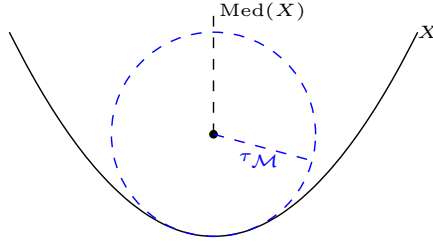


Figure 9: Geometric intuition of reach.

The characterization of reach as the radius of the largest ambient tangent ball is used in our proof of Theorem 4 below. Theorem 1 holds by applying Theorem 4 to each chart U_i .

Theorem 4. *Let $\delta > 0$. Suppose $U \subset \mathbb{R}^D$ is a connected d -dimensional manifold such that $\|u_1 - u_2\| \leq 2\tau_U - \delta$ for all $u_1, u_2 \in U$. Then there is a d -dimensional affine space $\mathcal{H} \subset \mathbb{R}^D$ such that the projection map $\pi_{\mathcal{H}} : U \rightarrow \mathcal{H}$ is bi-Lipschitz with lower Lipschitz constant $(1 + (D - d)\frac{2\tau_U}{\delta})^{-1/2}$.*

Proof. We first prove the theorem in the case of a codimension 1 manifold, then leverage this result in the general case.

Case 1: *Suppose U is $(D - 1)$ -dimensional.*

Recall from the geometric intuition of reach in Figure 9 that an ambient ball of radius τ_U that lies tangent to U does not contain any points from U in its interior. Moreover, since $\|u_1 - u_2\| \leq 2\tau_U - \delta$ for all $u_1, u_2 \in U$, we can choose an ambient ball \mathcal{B} of radius τ_U tangent to U such that U lies on one side of an affine hyperplane \mathcal{H} that intersects \mathcal{B} to create chords of length bounded by $2\tau_U - \delta$, as shown in Figure 10.

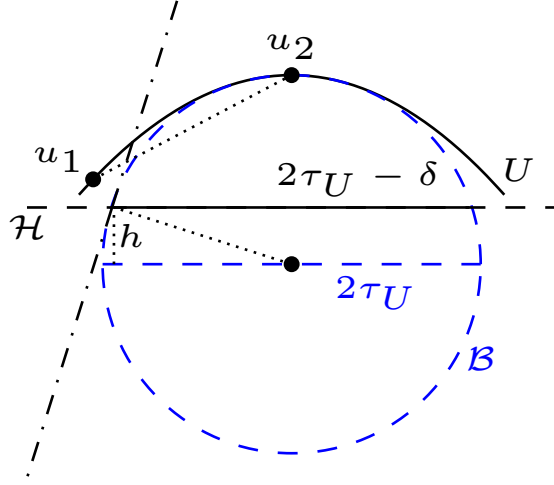


Figure 10: A 2-dimensional slice of an ambient tangent ball of radius τ_U , chosen so that U lies above the hyperplane \mathcal{H} which intersects \mathcal{B} with chord length $2\tau_U - \delta$.

Let $\{v_1, \dots, v_{D-1}\}$ be an orthonormal basis for \mathcal{H} , and let \mathbf{n} be a unit vector normal to \mathcal{H} so that $\{v_1, \dots, v_{D-1}, \mathbf{n}\}$ is an orthonormal basis for \mathbb{R}^D . Given $u_1, u_2 \in U$, consider a 2-dimensional slice of \mathcal{B} and U parallel to $\pi_{\mathcal{H}}(u_1) - \pi_{\mathcal{H}}(u_2)$ and perpendicular to \mathcal{H} , as pictured in Figure 10. The slope of the secant line between u_1 and u_2 is $|\langle u_1 - u_2, \mathbf{n} \rangle| / \|\pi_{\mathcal{H}}(u_1) - \pi_{\mathcal{H}}(u_2)\|$. Moreover, the slope of this secant line is smaller in absolute value than the slope of the line tangent to \mathcal{B} at its intersection with \mathcal{H} . Indeed, if the slope of the secant line exceeded that of the tangent line, then there would be a geodesic $\gamma : [a, b] \rightarrow U$ of U such that $\|\gamma''(t)\| > \tau_U^{-1}$ for some t (i.e., the curvature of U would exceed τ_U^{-1} at some point which would mean that \mathcal{B} could not lie tangent to U at this point, contradicting the definition of τ_U). This tangent line has slope $(\tau_U - \delta/2)/h$, where h is the distance between \mathcal{H} and the parallel hyperplane that divides \mathcal{B} in half. Note that

$$h = \sqrt{\tau_U^2 - (\tau_U - \delta/2)^2} = \sqrt{\tau_U^2 - (\tau_U^2 - \delta\tau_U + \delta^2/4)} = \sqrt{\delta\tau_U - \delta^2/4}.$$

Moreover, since $\delta < 2\tau_U$ we have $\tau_U - \delta/4 > \tau_U - \tau_U/2 = \tau_U/2$, so

$$h = \sqrt{\delta\tau_U - \delta^2/4} = \sqrt{\delta(\tau_U - \delta/4)} > \sqrt{\delta\tau_U/2}.$$

Since the slope of the secant line between u_1 and u_2 is bounded by the slope of the aforementioned tangent line, we have

$$\frac{|\langle u_1 - u_2, \mathbf{n} \rangle|}{\|\pi_{\mathcal{H}}(u_1) - \pi_{\mathcal{H}}(u_2)\|} \leq \frac{\tau_U - \delta/2}{h} < \frac{\tau_U}{\sqrt{\delta\tau_U/2}} = \left(\frac{2\tau_U}{\delta}\right)^{1/2}.$$

Finally, since $\{v_1, \dots, v_{D-1}, \mathbf{n}\}$ is an orthonormal basis for \mathbb{R}^D , it follows that

$$\begin{aligned} \|u_1 - u_2\|^2 &= \sum_{i=1}^{D-1} |\langle u_1 - u_2, v_i \rangle|^2 + |\langle u_1 - u_2, \mathbf{n} \rangle|^2 \\ &= \|\pi_{\mathcal{H}}(u_1) - \pi_{\mathcal{H}}(u_2)\|^2 + |\langle u_1 - u_2, \mathbf{n} \rangle|^2 \\ &\leq \|\pi_{\mathcal{H}}(u_1) - \pi_{\mathcal{H}}(u_2)\|^2 + \left(\frac{2\tau_U}{\delta}\right) \|\pi_{\mathcal{H}}(u_1) - \pi_{\mathcal{H}}(u_2)\|^2 \\ &= \left(1 + \frac{2\tau_U}{\delta}\right) \|\pi_{\mathcal{H}}(u_1) - \pi_{\mathcal{H}}(u_2)\|^2. \end{aligned}$$

Therefore $\left(1 + \frac{2\tau_U}{\delta}\right)^{-1/2} \|u_1 - u_2\| \leq \|\pi_{\mathcal{H}}(u_1) - \pi_{\mathcal{H}}(u_2)\| \leq \|u_1 - u_2\|$, so $\pi_{\mathcal{H}}$ is bi-Lipschitz.

Case 2: Suppose U is d -dimensional with $1 \leq d < D - 1$.

Begin by choosing an ambient ball \mathcal{B} of radius τ_U that lies tangent to U such that U lies on one side of a $(D - 1)$ -dimensional hyperplane \mathcal{H}_1 that intersects \mathcal{B} to create chords of length bounded by $2\tau_U - \delta$, as in Case 1 (this is still possible because of the condition $\|u_1 - u_2\| \leq 2\tau_U - \delta$ for all $u_1, u_2 \in U$). Let \mathbf{n}_1 denote the normal vector of \mathcal{H}_1 . Next, choose any $(D - 1)$ -dimensional hyperplane $\hat{\mathcal{H}}_2$ that is orthogonal to \mathcal{H}_1 . Again by the condition $\|u_1 - u_2\| \leq 2\tau_U - \delta$ for all $u_1, u_2 \in U$, there exists an orthogonal matrix Q_1 such that $Q_1 \mathbf{n}_1 = \mathbf{n}_1$ and U lies on one side of $\mathcal{H}_2 = Q_1 \hat{\mathcal{H}}_2$. Let \mathbf{n}_2 denote the unit normal vector of \mathcal{H}_2 . Continuing in this fashion, we can construct a sequence $\mathcal{H}_1, \dots, \mathcal{H}_{D-d}$ of mutually orthogonal hyperplanes of dimension $D - 1$ that each intersect an ambient ball tangent to U with chord length less than $2\tau_U - \delta$. Let $\mathbf{n}_1, \dots, \mathbf{n}_{D-d}$ denote the unit normal vectors of these hyperplanes. Next, define

$$\mathcal{H} = \bigcap_{k=1}^{D-d} \mathcal{H}_k.$$

Since each \mathcal{H}_k is $(D - 1)$ -dimensional and orthogonal, \mathcal{H} is d -dimensional. Let $\{v_1, \dots, v_d\}$ be an orthonormal basis for \mathcal{H} so that $\{v_1, \dots, v_d, \mathbf{n}_1, \dots, \mathbf{n}_{D-d}\}$ is an orthonormal basis for \mathbb{R}^D . Given $u_1, u_2 \in U$ and $k \in \{1, \dots, D - d\}$, consider the 2-dimensional slice of \mathbb{R}^D parallel to $\pi_{\mathcal{H}}(u_1) - \pi_{\mathcal{H}}(u_2)$ and \mathbf{n}_k . As in Case 1, we see that $|\langle u_1 - u_2, \mathbf{n}_k \rangle|^2 \leq \left(\frac{2\tau_U}{\delta}\right) \|\pi_{\mathcal{H}}(u_1) - \pi_{\mathcal{H}}(u_2)\|^2$. It follows that

$$\begin{aligned} \|u_1 - u_2\|^2 &= \sum_{i=1}^d |\langle u_1 - u_2, v_i \rangle|^2 + \sum_{k=1}^{D-d} |\langle u_1 - u_2, \mathbf{n}_k \rangle|^2 \\ &= \|\pi_{\mathcal{H}}(u_1) - \pi_{\mathcal{H}}(u_2)\|^2 + \sum_{k=1}^{D-d} |\langle u_1 - u_2, \mathbf{n}_k \rangle|^2 \\ &\leq \|\pi_{\mathcal{H}}(u_1) - \pi_{\mathcal{H}}(u_2)\|^2 + (D - d) \left(\frac{2\tau_U}{\delta}\right) \|\pi_{\mathcal{H}}(u_1) - \pi_{\mathcal{H}}(u_2)\|^2 \\ &= \left(1 + (D - d) \frac{2\tau_U}{\delta}\right) \|\pi_{\mathcal{H}}(u_1) - \pi_{\mathcal{H}}(u_2)\|^2. \end{aligned}$$

Therefore $\left(1 + (D - d) \frac{2\tau_U}{\delta}\right)^{-1/2} \|u_1 - u_2\| \leq \|\pi_{\mathcal{H}}(u_1) - \pi_{\mathcal{H}}(u_2)\| \leq \|u_1 - u_2\|$, so $\pi_{\mathcal{H}}$ is bi-Lipschitz. \square

B.2 Proof of Theorem 2

Since the atlas $\{(U_i, \phi_i)\}_{i=1}^n$ is a finite distortion embedding of \mathcal{M} , each decoder $D_i = \phi_i^{-1}|_{\phi_i(U_i)} : \phi_i(U_i) \rightarrow \mathbb{R}^D$ is Lipschitz. Thus, Theorem 2 holds by the following result, with the additional observation that only the final layer depends on the ambient dimension D of the manifold.

Theorem 5. *Let $f : \mathbb{R}[0, 1]^d \rightarrow \mathbb{R}^D$ be bounded and Lipschitz. Then for any $\epsilon \in (0, 1)$, there is a ReLU network \tilde{f} such that*

1. $\|f - \tilde{f}\|_\infty < \epsilon$;
2. \tilde{f} has at most $c \ln(1/\epsilon) + 1$ layers and $c\epsilon^{-d}(\ln(1/\epsilon) + D)$ computation units, for some constant $c = c(d)$.

Proof. For a positive integer N , let $\{\varphi_{\mathbf{m}}\}_{\mathbf{m} \in \{0, 1, \dots, N\}^d}$ be the partition of unity on the domain $[0, 1]^d$ defined on a grid of $(N + 1)^d$ points as in [45]:

$$\varphi_{\mathbf{m}}(\mathbf{x}) = \prod_{k=1}^d \psi(3Nx_k - m_k), \quad (3)$$

where

$$\psi(x) = \begin{cases} 1, & |x| < 1, \\ 0, & 2 < |x|, \\ 2 - |x|, & 1 \leq |x| \leq 2. \end{cases} \quad (4)$$

Define

$$\hat{f} = \sum_{\mathbf{m}} \varphi_{\mathbf{m}} f\left(\frac{\mathbf{m}}{N}\right), \quad (5)$$

a sum-product of the partition of unity with constant functions equal to f evaluated at each grid point $\mathbf{x} = \frac{\mathbf{m}}{N}$. Then

$$\begin{aligned} \|f(x) - \hat{f}(x)\| &= \left\| \sum_{\mathbf{m}} \varphi_{\mathbf{m}}(\mathbf{x}) (f(\mathbf{x}) - f(\frac{\mathbf{m}}{N})) \right\| \\ &\leq \sum_{\mathbf{m}} |\varphi_{\mathbf{m}}(\mathbf{x})| \|f(\mathbf{x}) - f(\frac{\mathbf{m}}{N})\| \\ &\leq \sum_{\mathbf{m}: |x_k - \frac{m_k}{N}| < \frac{1}{N} \forall k} \|f(\mathbf{x}) - f(\frac{\mathbf{m}}{N})\| \\ &\leq 2^d \max_{\mathbf{m}: |x_k - \frac{m_k}{N}| < \frac{1}{N} \forall k} \|f(\mathbf{x}) - f(\frac{\mathbf{m}}{N})\| \end{aligned}$$

since $\text{supp } \varphi_{\mathbf{m}} = \{\mathbf{x} : |x_k - \frac{m_k}{N}| < \frac{1}{N} \forall k\}$ and each \mathbf{x} belongs to the support of at most 2^d functions $\varphi_{\mathbf{m}}$. Applying Taylor's theorem to $\|f(\mathbf{x}) - f(\frac{\mathbf{m}}{N})\|$, we get

$$\|f(x) - \hat{f}(x)\| \leq 2^d \frac{\sqrt{d}}{N} \text{ess sup}_{\mathbf{x} \in [0, 1]^d} \|J_f(\mathbf{x})\| \leq \frac{2^d L \sqrt{d}}{N} \quad (6)$$

where L is the Lipschitz constant of f , since $\|\mathbf{x} - \frac{\mathbf{m}}{N}\| \leq \frac{\sqrt{d}}{N}$ for all $\mathbf{x} \in \text{supp } \varphi_{\mathbf{m}}$. Thus, if we choose

$$N > \frac{2^{d+1} L \sqrt{d}}{\epsilon} \quad (7)$$

then

$$\|f - \hat{f}\|_\infty \leq \frac{\epsilon}{2}. \quad (8)$$

We will now approximate

$$\hat{f}(\mathbf{x}) = \sum_{\mathbf{m}} \varphi_{\mathbf{m}}(\mathbf{x}) f\left(\frac{\mathbf{m}}{N}\right)$$

with a neural network. By Proposition 3 in [45], given $K > 0$ and $\delta \in (0, 1)$, there exists a ReLU network η that implements a “multiplication” function $\tilde{\times} : \mathbb{R}^2 \rightarrow \mathbb{R}$ such that $|\tilde{\times}(x, y) - xy| \leq \delta$ whenever $|x| \leq K$ and $|y| \leq K$, $\tilde{\times}(x, y) = 0$ whenever $x = 0$ or $y = 0$, and the number of layers and computation units in η is at most $c_1 \ln(1/\delta) + c_2$, where $c_2 = c_2(K)$. For each $\mathbf{m} \in \{0, 1, \dots, N\}^d$, define

$$\tilde{\varphi}_{\mathbf{m}}(\mathbf{x}) = \tilde{\times}(\psi(3Nx_1 - m_1), \tilde{\times}(\psi(3Nx_2 - m_2), \dots)), \quad (9)$$

which includes $d - 1$ applications of $\tilde{\times}$. Since $|\psi(x)| \leq 1$, repeated application of the property $|\tilde{\times}(x, y)| \leq |x| \cdot |y| + \delta$ with $|x| \leq 1$ and $\delta < 1$ shows that each argument given to $\tilde{\times}$ in Equation (9) is bounded by $K = d$. It follows that $\tilde{\varphi}_{\mathbf{m}}$ can be implemented by a ReLU network with number of layers and units at most $c \ln(1/\delta)$ for some constant $c = c(d)$. Moreover, we have

$$\begin{aligned} |\tilde{\varphi}_{\mathbf{m}}(\mathbf{x}) - \varphi_{\mathbf{m}}(\mathbf{x})| &= |\tilde{\times}(\psi(3Nx_1 - m_1), \tilde{\times}(\psi(3Nx_2 - m_2), \dots)) - \psi(3Nx_1 - m_1)\psi(3Nx_2 - m_2) \cdots| \\ &\leq |\tilde{\times}(\psi(3Nx_1 - m_1), \tilde{\times}(\psi(3Nx_2 - m_2), \tilde{\times}(\psi(3Nx_3 - m_3), \dots))) \\ &\quad - \psi(3Nx_1 - m_1) \cdot \tilde{\times}(\psi(3Nx_2 - m_2), \tilde{\times}(\psi(3Nx_3 - m_3), \dots))| \\ &\quad + |\psi(3Nx_1 - m_1)| \cdot |\tilde{\times}(\psi(3Nx_2 - m_2), \tilde{\times}(\psi(3Nx_3 - m_3), \dots)) \\ &\quad - \psi(3Nx_2 - m_2) \cdot \tilde{\times}(\psi(3Nx_3 - m_3), \dots)| \\ &\quad + \dots \\ &\leq d\delta \end{aligned}$$

since $|\tilde{\times}(x, y) - xy| \leq \delta$ and $|\psi(x)| \leq 1$. Additionally, $\tilde{\varphi}_{\mathbf{m}}(\mathbf{x}) = \varphi_{\mathbf{m}}(\mathbf{x}) = 0$ for $\mathbf{x} \notin \text{supp } \varphi_{\mathbf{m}}$ since $\tilde{\times}(x, y) = 0$ whenever $x = 0$ or $y = 0$. Thus, if we define

$$\tilde{f}(\mathbf{x}) = \sum_{\mathbf{m}} \tilde{\varphi}_{\mathbf{m}}(\mathbf{x}) f\left(\frac{\mathbf{m}}{N}\right) \quad (10)$$

then

$$\begin{aligned} \|\tilde{f}(\mathbf{x}) - \hat{f}(\mathbf{x})\| &= \left\| \sum_{\mathbf{m}} (\tilde{\varphi}_{\mathbf{m}}(\mathbf{x}) - \varphi_{\mathbf{m}}(\mathbf{x})) f\left(\frac{\mathbf{m}}{N}\right) \right\| \\ &= \left\| \sum_{\mathbf{m}: \mathbf{x} \in \text{supp } \varphi_{\mathbf{m}}} (\tilde{\varphi}_{\mathbf{m}}(\mathbf{x}) - \varphi_{\mathbf{m}}(\mathbf{x})) f\left(\frac{\mathbf{m}}{N}\right) \right\| \\ &\leq 2^d M \max_{\mathbf{m}: \mathbf{x} \in \text{supp } \varphi_{\mathbf{m}}} |\tilde{\varphi}_{\mathbf{m}}(\mathbf{x}) - \varphi_{\mathbf{m}}(\mathbf{x})| \\ &\leq 2^d M d \delta \end{aligned}$$

where M is an upper bound for f . If we set

$$\delta = \frac{\epsilon}{2^{d+1} M d} \quad (11)$$

then $\|\tilde{f}(\mathbf{x}) - \hat{f}(\mathbf{x})\| \leq \frac{\epsilon}{2}$, and hence

$$\|f - \tilde{f}\|_\infty \leq \epsilon. \quad (12)$$

Finally, \tilde{f} can be implemented as one ReLU network consisting of $(N+1)^d$ parallel subnetworks $\tilde{\varphi}_{\mathbf{m}}$, with a final D -by- $(N+1)^d$ layer of weights $f\left(\frac{\mathbf{m}}{N}\right)$. This results in an overall network with at most $c \ln(1/\delta) + 1$ layers and $(N+1)^d(c \ln(1/\delta) + D)$ weights. With N given by (7) and δ given by (11), we get our desired complexity bounds of $c \ln(1/\epsilon) + 1$ layers and $c\epsilon^{-d}(\ln(1/\epsilon) + D)$ computation units. \square

B.3 Proof of Theorem 3

Since the atlas $\{(U_i, \phi_i)\}_{i=1}^n$ is a finite distortion embedding of \mathcal{M} , each decoder $D_i = \phi_i^{-1}|_{\phi_i(U_i)} : \phi_i(U_i) \rightarrow \mathbb{R}^D$ is C^k and Lipschitz. Thus, Theorem 3 holds by the following result. For this section, we assume $X \in \mathbb{R}^d$ has density bounded away from 0 and $\|\text{cov}(Y - f(X)|X = x)\| \leq \sqrt{c/D}$ for some constant c .

Theorem 6. *Let $f : \mathbb{R}[0, 1]^d \rightarrow \mathbb{R}^D$ satisfy $f \in C^k([0, 1]^d)$ and be Lipschitz with constant L . Given an i.i.d. sample $\{x_i, y_i\}_{i=1}^n$ from (X, Y) satisfying the sampling assumptions above, define the approximation \hat{f}_n as in (14). Then for any $\epsilon > 0$ there are C and n large enough so that*

$$P(2^d \cdot \|f - \hat{f}_n\|_\infty > Cn^{-\frac{k}{2k+d}} + L\sqrt{d}N^{-1}) \leq \epsilon.$$

Proof. Let $f : \mathbb{R}[0, 1]^d \rightarrow \mathbb{R}^D$ such that $f \in C^k([0, 1]^d)$ and f is Lipschitz with constant L . Let $\{\varphi_{\mathbf{m}}\}_{\mathbf{m} \in \{0, \dots, N\}^d}$ be the piecewise partition of unity introduced in [45] and discussed in Appendix B.2. Given an i.i.d. sample $\{x_i, y_i\}_{i=1}^n$ from (X, Y) , at each grid point $\mathbf{x}_{\mathbf{m}} = \frac{\mathbf{m}}{N} \in [0, 1]^d$, solve the local polynomial regression problem

$$\pi_{\mathbf{m}, n}^*(\mathbf{x}) = \arg \min_{\pi \in \Pi_{k-1}^{d \rightarrow D}} \frac{1}{|I_{\mathbf{m}, n}|} \sum_{i \in I_{\mathbf{m}, n}} \|y_i - \pi(x_i - \mathbf{x}_{\mathbf{m}})\|^2 \quad (13)$$

where $I_{\mathbf{m}, n} = \{i \mid \|x_i - \mathbf{x}_{\mathbf{m}}\| \leq N^{-1}\}$ and N satisfies $0 < \lim_{n \rightarrow \infty} n^{\frac{1}{2k+d}} N^{-1} < \infty$ as in [2]. Next, let $\bar{\pi}_{\mathbf{m}, n}$ denote the constant term of each regression function $\pi_{\mathbf{m}, n}^*$ and define

$$\hat{f}_n(\mathbf{x}) = \sum_{\mathbf{m}} \varphi_{\mathbf{m}}(\mathbf{x}) \bar{\pi}_{\mathbf{m}, n}. \quad (14)$$

Then

$$\begin{aligned} \|f(\mathbf{x}) - \hat{f}_n(\mathbf{x})\| &= \left\| \sum_{\mathbf{m}} \varphi_{\mathbf{m}}(\mathbf{x}) (f(\mathbf{x}) - \bar{\pi}_{\mathbf{m}, n}) \right\| \\ &\leq \sum_{\mathbf{m}: |x_k - \frac{m_k}{N}| < \frac{1}{N} \forall k} |\varphi_{\mathbf{m}}(\mathbf{x})| \|f(\mathbf{x}) - \bar{\pi}_{\mathbf{m}, n}\| \\ &\leq \sum_{\mathbf{m}: |x_k - \frac{m_k}{N}| < \frac{1}{N} \forall k} \|f(\mathbf{x}) - \bar{\pi}_{\mathbf{m}, n}\| \\ &\leq 2^d \max_{\mathbf{m}: |x_k - \frac{m_k}{N}| < \frac{1}{N} \forall k} \|f(\mathbf{x}) - \bar{\pi}_{\mathbf{m}, n}\|. \end{aligned}$$

since $\text{supp } \varphi_{\mathbf{m}} = \{\mathbf{x} : |x_k - \frac{m_k}{N}| < \frac{1}{N} \forall k\}$ and each \mathbf{x} belongs to the support of at most 2^d functions $\varphi_{\mathbf{m}}$. Next, we write

$$\|f(\mathbf{x}) - \bar{\pi}_{\mathbf{m},n}\| \leq \|f(\mathbf{x}) - f(\mathbf{x}_{\mathbf{m}})\| + \|f(\mathbf{x}_{\mathbf{m}}) - \bar{\pi}_{\mathbf{m},n}\|.$$

For all $\mathbf{x} \in \text{supp } \varphi_{\mathbf{m}}$, we have

$$\|f(\mathbf{x}) - f(\mathbf{x}_{\mathbf{m}})\| \leq L\|\mathbf{x} - \mathbf{x}_{\mathbf{m}}\| \leq \frac{L\sqrt{d}}{N}$$

since $|x_k - \frac{m_k}{N}| < \frac{1}{N} \forall k$ implies $\|\mathbf{x} - \mathbf{x}_{\mathbf{m}}\| \leq \frac{\sqrt{d}}{N}$. For the second term, given $\delta > 0$ there exist C and n large enough so that

$$P(\|f(\mathbf{x}_{\mathbf{m}}) - \bar{\pi}_{\mathbf{m},n}\| > Cn^{-\frac{k}{2k+d}}) \leq \delta$$

by [2]. Since the uncertainty only occurs at the $(N+1)^d$ grid points $\mathbf{x}_{\mathbf{m}}$, we can take a finite union bound to get

$$P\left(\max_{\mathbf{x} \in \text{supp } \varphi_{\mathbf{m}}} \|f(\mathbf{x}) - \bar{\pi}_{\mathbf{m},n}\| > Cn^{-\frac{k}{2k+d}} + L\sqrt{d}N^{-1}\right) \leq (N+1)^d \delta.$$

Choosing C and n large enough so that $\delta \leq \frac{\epsilon}{(N+1)^d}$, it follows that

$$P(2^d \cdot \|f - \hat{f}_n\|_{\infty} > Cn^{-\frac{k}{2k+d}} + L\sqrt{d}N^{-1}) \leq \epsilon$$

as desired.

Finally, we note that \hat{f}_n can be approximated by a ReLU network similar to \tilde{f} in Appendix B.2, except the weights in the final layer are given by $\bar{\pi}_{\mathbf{m}}$, which are computed using known sample values instead of unknown function values $f(\frac{\mathbf{m}}{N})$. The parameter N controls the granularity of the partition of unity and in turn the width of the network that approximates \hat{f}_n . \square